RANKS OF ELLIPTIC CURVES AND DEEP NEURAL NETWORKS

MATIJA KAZALICKI AND DOMAGOJ VLAH

1. Abstract

Determining the rank of an elliptic curve $E/\mathbb{Q}$ is a difficult problem. In applications such as the search for curves of high rank, one often relies on heuristics to estimate the analytic rank (which is equal to the rank under the Birch and Swinnerton-Dyer conjecture).

In this paper, we propose a novel rank classification method based on deep convolutional neural networks (CNNs). The method takes as input the conductor of E and a sequence of normalized Frobenius traces a_p for primes p in a certain range ($p < 10^k$ for $k = 3, 4, 5$), and aims to predict the rank or detect curves of "high" rank. We compare our method with eight simple neural network models of the Mestre-Nagao sums, which are widely used heuristics for estimating the rank of elliptic curves.

We evaluate our method on two datasets: the LMFDB and a custom dataset consisting of elliptic curves with trivial torsion, conductor up to 10^{30}, and rank up to 10. Our experiments demonstrate that the CNNs outperform the Mestre-Nagao sums on the LMFDB dataset (remarkably, the neural network that took as an input all Mestre-Nagao sums performed much better than each sum individually). On the custom dataset, the performance of the CNNs and the Mestre-Nagao sums is comparable.

2. Introduction

Let E be an elliptic curve over $\mathbb{Q}$ with discriminant Δ and conductor N. A celebrated theorem of Mordell states that the group of rational points $E(\mathbb{Q})$ is a finitely generated abelian group isomorphic to $E(\mathbb{Q})_{\text{tors}} \times \mathbb{Z}^r$, where $E(\mathbb{Q})_{\text{tors}}$ is the torsion subgroup of $E(\mathbb{Q})$ and r is the rank of $E(\mathbb{Q})$. While the possible torsion subgroups were completely classified by Mazur [Maz77] and easy to compute, the rank of the elliptic curve is a much more mysterious quantity. Not only it is not known which values can be obtained as ranks (although this question was already asked by Poincaré [Poi01]), there is also no agreement on whether the rank is unbounded or not. Up until recently, the folklore conjecture was that the rank is unbounded which was challenged by the series of papers [WDE$^+$14, Wat15, PPVW19] that predict (based on different heuristic models) that there are only finitely many elliptic curves with rank greater than 21. The current rank record is 28 by Elkies [Elk06]. For more information about the rank records for curves with fixed torsion subgroups as well for rank in families, see [Duj].

The search for curves of high rank is challenging, partly because determining the rank of an elliptic curve is a computationally expensive task. Also, there is no algorithm known to correctly compute the rank in all cases. This is mainly because finding rational points on elliptic curves is a difficult problem, and descent algorithms that are commonly used eventually reduce to a naive point search on some auxiliary curves. To overcome this difficulty, researchers use rank heuristics that are inspired by the Birch and Swinnerton-Dyer conjecture. These heuristics help in identifying probable candidates for elliptic curves of high rank, thereby reducing the computational burden of computing the rank of all curves.

For each prime of good reduction p, we define $a_p = p + 1 - \#E(\mathbb{F}_p)$. For $p|N$, we set $a_p = 0, -1$, or 1 if, respectively, E has additive, split multiplicative or non-split multiplicative reduction at p. The L-function attached to $E/\mathbb{Q}$ is then defined as an Euler product

$$L_E(s) = \prod_{p|\Delta} \left(1 - \frac{a_p}{p^s}\right)^{-1} \prod_{p\nmid\Delta} \left(1 - \frac{a_p}{p^s} + \frac{p}{p^{2s}}\right)^{-1},$$

which converges absolutely for $\Re(s) > 3/2$ and extends to an entire function by the Modularity theorem [Wil95, BCDT01]. The Birch and Swinnerton-Dyer (BSD) conjecture states that the order of vanishing of $L_E(s)$ at $s = 1$ (the quantity known as analytic rank) is equal to the rank of $E(\mathbb{Q})$.

Mestre [Mes82] and Nagao [Nag92], and later others [EK20, Bob13], motivated by BSD conjecture, considered certain sums (see Section 3 for the list of sums examined in this paper) which heuristically should be able to detect curves of high analytic rank. In an abuse of terminology, we refer to all such sums as the Mestre-Nagao sums. For example, one of these sums (see Section 2 in [EK20])

$$\tilde{S}_5(B) = \sum_{\substack{p<B,\\ \text{good reduction}}} \log\left(\frac{p+1-a_p}{p}\right)$$

has a property that $\exp(-\tilde{S}_5(B))$ is the partial product of $L_E(s)$

$$\prod_{\substack{p<B,\\ \text{good reduction}}} \left(1 - a_p p^{-s} + p^{1-2s}\right)^{-1}, \tag{2.1}$$

evaluated at $s = 1$ (ignoring the primes of bad reduction). One expects that $\tilde{S}_5(B)$ should be large if E has a large rank since then the partial product should rapidly approach zero. This sum was used in [EK20] as a first step in finding rank-record breaking curves with fixed cyclic torsion $\mathbb{Z}/n\mathbb{Z}$ for $n = 2, 3, \ldots 7$.

Recently, some new fundamental results have been discovered with the assistance of deep neural networks in topology and representation theory [DVB$^+$21], combinatorics [Wag21], as well as some applications to problems in statistics [IV21, IV23]. In number theory, the utility of machine learning methods was shown in [HLO23, HLOP22] where the authors, among other things, successfully used logistic regression for classifying elliptic curves of rank zero and one.

In this paper, we investigate a deep learning algorithm for rank classification based on convolutional neural networks (CNN). These networks take as an input the conductor of the elliptic curve together with the sequence of normalized a_p-s (i.e. $a_p/\sqrt{p}$) for p in a fixed range and output the rank of the elliptic curve. We compare its performance to that of the Mestre-Nagao sums $\{S_0, S_1, \ldots, S_6, \Omega\}$ (defined in Section 3). A priori, it is not clear how to decide on the rank of the elliptic curve based on the value of its Mestre-Nagao sum (see related question (1) in Section 7 of [EK20]), so we train a simple fully connected neural network to do that task for us. Since the answer critically depends on the conductor of the elliptic curve, these networks, besides the Mestre-Nagao sum, take the conductor of the elliptic curve as an input. Training these networks revealed the optimal cutoff of the specific Mestre-Nagao sum for rank classification (for cutoffs of S_5 see Figure 3).

Architecture and the training process of our neural networks are described in Section 5. For training, we used two datasets. One is the LMFDB database [LMF22] which contains $3,824,372$ elliptic curves defined over $\mathbb{Q}$, divided into $2,917,287$ isogeny classes, with rank between 0 and 5 and conductor less than $300,000,000$. For more information about the structure of LMFDB database (it consists of three distinct datasets) see Section 4.1. The other one is a custom-made dataset that consists of $2,033,965$ elliptic curves with trivial torsion, the conductor less than 10^{30}, and the rank in the range between 0 and 10. Although this dataset is biased and does not represent typical elliptic curves from a given rank and conductor range (because its high-rank elliptic curves have low height generators, for discussion see Section 4), it is useful for comparing different classification methods.

For each neural network (the CNN or one of the Mestre-Nagao sums, in total 9) we have performed 24 tests by varying

a) dataset - LMFDB or custom,
b) range of a_p-s - we considered $(a_p)_{p\leq B}$ for $B = 10^3, 10^4$, and 10^5,
c) test curves - uniformly selected (20% from the dataset) or all curves in the top conductor range (which is $[10^8, 10^9]$ for the LMFDB and $[10^{29}, 10^{30}]$ for the custom dataset),
d) type of classification - binary or all ranks (for the LMFDB the rank range is from 0 to 5, and for the custom dataset from 0 to 10).

In binary classification, curves are labeled as either of low or high rank. For the LMFDB high rank means rank 4 (we did not consider 19 rank 5 curves), while for custom dataset high rank is $8, 9$ or 10. Here, the idea is to test how good neural networks are in detecting elliptic curves of high rank.

The neural networks have been selected to maximize the Matthews correlation coefficient (MCC) or phi coefficient, which is generally regarded as a balanced measure of the quality of the classification even if the classes are of very different sizes [BJEA17], and

Type of classifier	Number of a_p-s used					
	LMFDB			custom dataset		
	$p < 10^3$	$p < 10^4$	$p < 10^5$	$p < 10^3$	$p < 10^4$	$p < 10^5$
CNN	0.9507	0.9958	0.9992	0.6129	0.7218	0.7958
S_5	0.6132	0.7774	0.8463	0.4987	0.5990	0.6696

Table 1. Comparison of the Matthews correlation coefficients of the CNN and S_5 all rank classifiers for the uniform test set.

thus prevents the classifier ignoring the small classes. This is relevant to our problem since elliptic curves of high rank are sparsely represented in our datasets (see Tables 2 and 4 for distribution of ranks in datasets). For binary classification, the MCC is computed using the following formula

$$MCC = \frac{TP \cdot TN - FP \cdot FN}{\sqrt{(TP + FP) \cdot (TP + FN) \cdot (TN + EP) \cdot (TN + FN)}},$$

where TP, FN, TN, FP denote, respectively, the number of true positives, false negatives, true negatives, and false positives. Note that MCC lies in the segment $[-1, 1]$ and $MCC = 1$ only in the case of perfect classification.

For a comparison of the Mathews correlation coefficients of the CNN and S_5 classifiers for the uniform test set, see Table 1.

In all the tests performed on the LMFDB dataset, the CNN outperformed the Mestre-Nagao sums (this is especially true in the classification of all ranks). For example, in the all ranks classification with $p < 10,000$ in the uniform range, the MCC of the CNN is 0.9958 (in particular, the CNN misclassified only 0.25% of the curves) while the best Mestre-Nagao sum S_2 has $MCC = 0.8697$ (it misclassified 8.1% of the curves). For more details see Table 6. Similarly, in the all ranks classification with $p < 10,000$ and top conductor range, the MCC of the CNN is 0.9289 (see confusion matrix in Figure 2) while the best Mestre-Nagao sum S_0 has $MCC = 0.5057$ (see Figure 4), which is remarkable!

We also trained a fully connected neural network Ω whose inputs were all Mestre-Nagao sums $\{S_0, \ldots, S_6\}$ (together with the conductor), and interestingly on the LMFDB dataset this network performed much better than any sum individually. For example, in the uniform range case above it attained $MCC = 0.9602$, and in the top range case $MCC = 0.7013$.

A binary classification on the LMFDB dataset (which tries to identify curves of rank 4) ended up being an easy task for both the CNN and the majority of the Mestre-Nagao sums - in a uniform mode they demonstrated the perfect classification even in $p < 1,000$ range (see Table 6 and 10).

Additionally, we evaluated trained models only on curves with prime conductors and curves with conductors lower than $500,000$, see Tables 7, 8, 9. Interestingly, we observed that curves with prime conductors are more challenging to classify.

The classification on the custom dataset was much more challenging for both the CNN and the Mestre-Nagao sums. For example, in all ranks classification with $p < 10,000$ and the uniform range, while the CNN with $MCC = 0.7218$ (it misclassified 23% of curves, while, for 3% of the curves prediction missed true rank for more than 1) still outperformed the best Mestre-Nagao sum S_1 with $MCC = 0.6890$ (it misclassified 26% of curves), it performed just a little bit better than the network Ω for which $MCC = 0.7069$ (see Table 11).

In the top conductor range (for all ranks classification on the custom dataset) all heuristics were much less efficient. This is expected, at least for the Mestre-Nagao sums, since the curves in this test set have large conductors (at least 10^{29}) and thus we need more a_p's to determine their L-function. The Mestre-Nagao sums slightly outperformed the CNN in this setting. For example, in $p < 10,000$ mode the MCC of the CNN was 0.3019 (it misclassified 61% of curves, while, for 12% of the curves prediction missed true rank for more than 1), while the best Mestre-Nagao sum S_2 had $MCC = 0.3291$. For complete information see Table 12.

In binary classification on the custom dataset (which tries to identify curves of rank $8, 9$ or 10), the CNN outperformed each Mestre-Nagao sum individually, but it was a little bit worse than the neural network trained on all Mestre-Nagao sums. For example, in the top conductor range for $p < 10,000$ the MCC of the CNN was 0.6774 while the MCC of all sums was 0.7091.

Next, we explore how the relationship between conductor N and the range of a_p used in the algorithm (we restrict to the set of a_p with $p < B$) influence the quality of classification. Understanding this relationship is important to properly assess the bound B required, for example, to successfully classify elliptic curves with conductors larger than those in our dataset (or to improve the classification of the curves in the current dataset).

We note that for any particular choice of a_p values with $p < B$, there is an infinite family of elliptic curves that realize them (as soon as there is one such curve). Since a_p depends only on the residue classes of the Weierstrass coefficients modulo p, the Weierstrass coefficients of the curves in this family can be easily described using the Chinese remainder theorem. However, one expects that the average rank (when curves are ordered by height) in this family, since it is determined by congruence constraints, will be $1/2$ (with 50% of curves having rank 0 and 50% having rank 1). Thus, the values of a_p in the range $p < B$ for a random curve from this family provide no useful information about its rank. In other words, if the conductor N is much larger than B, we do not expect classification to work.

As a toy model for detecting rank-0 curves, we can numerically evaluate $L_E(1)$ using the approximate functional equation (see Section 6 in [Coh15]) given by

$$L_E(1) = 2\sum_{n=1}^{\infty} \frac{a_n}{n} e^{-2\pi n/\sqrt{N}},$$

where a_n are the coefficients of the Dirichlet series $L_E(s) = \sum_{n=1}^{\infty} \frac{a_n}{n^s}$. To ensure a small error of the approximation, we require $B = \sqrt{N}$ at a minimum. Likewise, the numerical tests for the modularity of L-functions [Boo05] and the numerical methods for computing bad Euler factors of genus-two curves [BSS+16] necessitate at least $B = \sqrt{N}$ for proper functioning. Therefore, we investigate the dependence of the quality of classification of various models, as measured by the MCC, on the quantity $B/\sqrt{N}$.

Figure 7 illustrates that the quality of classification of the CNN, as a function of $B/\sqrt{N}$, is similar, although not identical, for all three trained models, where $B = 10^k$ for $k = 3, 4, 5$. This observation suggests that to maintain the quality of the classification when increasing the conductor N, the bound B should be increased to maintain a constant $B/\sqrt{N}$ value. Since the conductors in the custom dataset reach up to 10^{30}, it is not surprising that the model's predictions are worse on the custom dataset than they are on the LMFDB. This is because the ratio of $B/\sqrt{N}$ is much smaller in the custom dataset than it is in the LMFDB, where the curves have conductors less than $3 \cdot 10^8$. Figure 8 further demonstrates that the CNN outperforms the other classifiers consistently in all the considered ranges of $B/\sqrt{N}$.

Finally, we evaluated the performance of the CNN model with $B = 10^5$ on a dataset of 808 elliptic curves with conductors less than 10^{29}. These curves were sampled from the $K3$ elliptic surface with discriminant -163 given by equation (4.1), which was used by Elkies [Elk07] to obtain the rank 12 elliptic curve with $\mathbb{Z}/4\mathbb{Z}$ torsion subgroup. This family has Mordell-Weil rank 4 and $\mathbb{Z}/4\mathbb{Z}$ torsion subgroup. Despite not being trained on curves with nontrivial torsion subgroups, the CNN model successfully classified curves of rank 6 and 7, as shown in the confusion matrix in Figure 9. The MCC of the CNN model was 0.2492.

3. Mestre-Nagao sums

In this section, we define and motivate the Mestre-Nagao sums that we are going to use for rank classification.

Let

$$\Lambda(n) = \begin{cases} \log p & \text{if } n = p^m, \\ 0 & \text{otherwise,} \end{cases}$$

be the von Mangoldt function, and for elliptic curve E defined over $\mathbb{Q}$ with conductor N_E let

$$c_n = \begin{cases} \alpha_p^m + \beta_p^m, & \text{if } n = p^m \text{ and } p \nmid N_E, \\ a_p^m, & \text{if } n = p^m \text{ and } p | N_E, \\ 0, & \text{otherwise,} \end{cases}$$

where α_p and β_p, for $p \nmid N_E$, are eigenvalues of the Frobenius morphism at p (thus $a_p = \alpha_p + \beta_p$ and $\alpha_p\beta_p = p$). Note that for $m > 1$ we have

$$\alpha_p^m + \beta_p^m = (\alpha_p^{m-1} + \beta_p^{m-1})a_p - p(\alpha_p^{m-2} + \beta_p^{m-2}),$$

hence for $p \nmid N_E$ it follows $c_{p^m} = c_{p^{m-1}}a_p - pc_{p^{m-1}}$. These number are related to analytic rank r_{an} of elliptic curve $E/\mathbb{Q}$ by a Laurent expansion of the logarithmic derivative of $L_E(s)$ around the point $s = 1$

$$-\frac{L_E'(s)}{L_E(s)} = \sum_{n=1}^{\infty} \frac{c_n\Lambda(n)}{n^s} = \frac{r_{an}}{s-1} + O(1).$$

We consider the following Mestre - Nagao sums.

$$S_0(B) = \frac{1}{\log B} \sum_{\substack{p<B,\\ \text{good reduction}}} \frac{a_p(E)\log p}{p},$$

$$S_1(B) = S_0(B) - \frac{1}{B\log B}\sum_{n\le B} c_n\Lambda(n),$$

$$S_2(B) = \frac{1}{\log B}\sum_{n\le B}\frac{c_n\Lambda(n)}{n} - \frac{1}{B\log B}\sum_{n\le B} c_n\Lambda(n),$$

$$S_3(B) = \sum_{\substack{p<B,\\ \text{good reduction}}} \frac{-a_p(E)+2}{p+1-a_p(E)}\log p,$$

$$S_4(B) = \frac{1}{B}\sum_{\substack{p<B,\\ \text{good reduction}}} -a_p(E)\log p,$$

$$S_5(B) = \sum_{\substack{p<B,\\ \text{good reduction}}} \log\left(\frac{p+1-a_p(E)}{p}\right) + \sum_{\substack{p<B,\\ \text{split mult. reduction}}} \log\left(3/2\cdot\frac{p-1}{p}\right),$$

$$S_6(D) = \frac{\log N_E}{2D\pi} - \frac{\log 2\pi}{D\pi} + \frac{-1}{D\pi}\sum_{p\le\exp(2\pi D)}\log p \sum_{k=1}^{\lfloor 2\pi D/\log p\rfloor}\frac{c_{p^k}}{p^{k/2}}\left(1-\frac{k\log p}{2\pi D}\right)$$
$$+\frac{1}{\pi}\Re\left\{\int_{-\infty}^{\infty}\frac{\Gamma'}{\Gamma}(1+it)\left(\frac{\sin(D\pi t)}{D\pi t}\right)^2 dt\right\}.$$

The sum S_0 was analyzed in detail in [KM22], where it was shown that if the Riemann hypothesis for $L_E(s)$ is true, and if the limit $\lim_{B\to\infty} S_0(B)$ exists, then the limit is $-r_{an} + 1/2$ where r_{an} is the analytic rank of $E/\mathbb{Q}$. The relation between S_0 and the analytic rank comes from Perron's formula applied to

$$\frac{1}{2\pi i}\int -\frac{L_E'(s)}{L_E(s)}\frac{x^s}{s(s-1)}ds, \quad x>1,\, d>3/2,\, a\in\mathbb{R}.$$

From the proof of Theorem 6. in [KM22], by modifying the error term of $S_0(B)$ one obtains sums S_1 and S_2 (equations (3.11) and (3.12)) that have essentially the same limit as S_0, but faster convergence.

Sums S_3 and S_4 were considered by Nagao [Nag92]. Note that $S_3(B)$ is the logarithmic derivative of the partial Euler product (2.1) evaluated at $s=1$ (ignoring the primes of bad reduction). Since $\frac{L_E'(s)}{L_E(s)}=\frac{r_{an}}{s-1}+O(1)$, it is reasonable to assume that for elliptic curve with large analytic rank r_{an}, the corresponding S_3 sum will be large (see Section 1.3.3 in [Cam99]). Sum S_5 is the modification of $\tilde{S_5}$ (from the introduction) at primes of split multiplicative reduction (see Section 7. in [EK20]).

Sum S_6 is described in [Bob13]. It is based on the explicit formula for $L_E(s)$ relating $S_6(D)$ to the sum over nontrivial zeros (with multiplicities) $\frac{1}{2}+i\gamma$ of $L_E(s)$, $\sum_\gamma f(\gamma)$, where $f(z)=f(z;D)=\left(\frac{\sin(D\pi z)}{D\pi z}\right)^2$. Note that $f(0)=1$ and $f(x)\geq 0$ for all real x, thus, $\sum_\gamma f(\gamma)$ gives an upper bound for r_{an}. Assuming Riemann Hypothesis for $L_E(s)$, one has $\lim_{D\to\infty} S_6(D)=r_{an}$, but computing $S_6(D)$ becomes infeasible once D gets a little larger than 4.4. For example, already to compute $S_6(2)$ one needs a_p's for all $p<286,751$.

For computing $S_6(D)$ we used C version [KS08] of PSAGE [S$^+$11] rankbound algorithm by Bober.

4. Datasets

We trained our models on two datasets, namely the LMFDB and the custom dataset. Furthermore, we evaluated the performance of the models on the dataset of elliptic curves sampled from the K3 elliptic surface given by equation (4.1).

4.1. **LMFDB.** The LMFDB database [LMF22] contains $3,824,372$ elliptic curves defined over $\mathbb{Q}$, distributed in $2,917,287$ isogeny classes. The LMFDB database is a union of three distinct datasets: all curves of conductor less than $500,000$, all curves whose conductor is 7-smooth, and all curves of prime conductor $p\leq 200,000,000$. We selected one representative per isogeny class, as curves in the same isogeny class have the same L-functions and hence the same analytic rank (but not necessarily the same torsion subgroup). Since there are only 19 curves with a rank equal to 5, we didn't take any of them into consideration. See Table 2 for rank distribution. Moreover, 63.71% of curves have trivial torsion, while 31.18% have $\mathbb{Z}/2\mathbb{Z}$ torsion.

4.2. **Custom dataset.** Our custom dataset contains $2,074,863$ elliptic curves defined over $\mathbb{Q}$ with trivial torsion and conductor less than 10^{30}. See Table 3 for the number

rank	0	1	2	3	4	5
count	1,404,510	1,887,132	493,291	37,334	2,086	19
proportion	36.73%	49.34%	12.90%	0.98%	0.05%	0.00%

Table 2. Distribution of ranks in the LMFDB dataset.

range	$[1, 10^5]$	$[10^5, 10^{10}]$	$[10^{10}, 10^{15}]$	$[10^{15}, 10^{20}]$	$[10^{20}, 10^{25}]$	$[10^{25}, 10^{29}]$	$[10^{29}, 10^{30}]$
proportion	0.94%	21.60%	26.97%	21.27%	17.02%	10.19%	1.97%

Table 3. Distribution of conductors in the custom dataset.

rank	0	1	2	3	4	5	6	7	8	9	10
count	$78,755$	$121,966$	$179,593$	$435,195$	$543,713$	$405,129$	$210,439$	$77,923$	$19,272$	$2,670$	201
proportion	3.79%	5.87%	8.65%	20.97%	26.20%	19.52%	10.14%	3.75%	0.92%	0.12%	0.01%

Table 4. Distribution of ranks in the custom dataset.

of curves in a specific conductor range. Our curves have rank between 0 and 10. See Table 4 for the distribution of curves by rank.

We used two methods for generating the dataset. First, we produced curves with random Weierstrass coefficients. These were primarily curves of rank 0 and 1.

The curves of higher rank were obtained as random specializations of pencils of cubics through randomly selected k rational points in the plane, for $k = 2, 3, \ldots, 8$. Every such cubic (if nonsingular) was transformed to Weierstrass form by the change of variables described in Chapter 8 of [Cas91]. We removed curves with nontrivial torsion subgroups.

Next, using PARI/GP [Par19] function ellrank we tried to compute ranks of all previously generated curves (assuming the Parity conjecture). Ultimately, we discarded those for which PARI/GP couldn't find the rank. Note that ellrank in computing the upper bound for the rank of the elliptic curve E approximates the rank of $\text{Ш}(E/\mathbb{Q})[2]$ from below with the rank of $\text{Ш}(E/\mathbb{Q})[2]/2\text{Ш}(E/\mathbb{Q})[4]$ (which it computes via Cassels pairing), thus it can not determine the rank of E if $\text{Ш}(E)[4]$ is nontrivial. Consequently, such curves are missing from our dataset.

It is important to note that this dataset suffers from bias as it is constructed by sampling the rational points of small height in the pencil of cubics. Consequently, it contains many elliptic curves with small canonical height generators and hence small regulators. This presents a problem, particularly for curves of small rank and large conductor, since the regulator is typically expected to be large under standard conjectures.

range	$[1, 10^5]$	$[10^5, 10^{10}]$	$[10^{10}, 10^{15}]$	$[10^{15}, 10^{20}]$	$[10^{20}, 10^{25}]$	$[10^{25}, 10^{29}]$
proportion	0.12%	0.49%	1.61%	7.30%	26.86%	63.61%

Table 5. Distribution of conductors in the K3 elliptic surface dataset.

The size of the regulator is significant since the Mestre-Nagao sums ultimately approximate a term whose size depends on both the rank and the regulator. For instance, from the original Birch and Swinnerton-Dyer conjecture,

$$\prod_{\substack{p<B,\\ \text{good reduction}}} \frac{p+1-a_p}{p} \approx A \log(B)^r,$$

it follows (by taking logarithms) that $\tilde{S}_5(B) = \log A + r \log\log B + o(1)$, where A is a constant that conjecturally depends on the regulator of E (e.g. see [Gol82]).

While this dataset does not represent typical elliptic curves of a given rank and conductor range, it is still helpful for comparing different classification methods.

4.3. **K3 elliptic surface.** Consider the K3 elliptic surface with discriminant -163 (see [Elk07, DP21])

$$\begin{aligned} y^2 = x^3 &+ (65536t^4 - 17472t^3 - 10176t^2 + 18672t - 3535)x^2 \\ &+ 1024(t+1)^2(15t-8)^2(31t-7)^2 x, \end{aligned} \tag{4.1}$$

of Mordell-Weil rank 4 (over $\mathbb{Q}(t)$) with $\mathbb{Z}/4\mathbb{Z}$ torsion subgroup. Generators of the infinite part of the Mordell-Weil group are points with x-coordinates

$$\begin{aligned} x_1 &= -361(t+1)(31t-7), \\ x_2 &= -4(t+1)(15t-8)(16t-7)^2, \\ x_3 &= -16(t+1)(8t+7)^2(15t-8), \\ x_4 &= 4(15t-8)(16t+1)^2(31t-7), \end{aligned}$$

while the point of order 4 has x-coordinate equal to $32(t+1)(15t-8)(31t-7)$.

To generate a sample of curves from this family, we substituted t with an integer between -2000 and 2000, resulting in 808 curves with conductors less than 10^{29}. However, we had to discard 37 curves because we were unable to compute their rank. The distribution of conductors in the dataset is given in Table 5.

5. Neural network architectures and training procedure

The models we employ are convolutional neural networks (CNN) [GBC16, II.9]. The CNN could be regarded as the composition of functions, so-called layers. Each layer is in principle composition of a fittable affine mapping and an element-wise nonlinear function. To detect and utilize any correlations in a_p sequence inherent to our data, for the affine mapping we use 1D matrix convolutional operations, inspired by the success of 2D matrix convolutions in image classification task [KSH12]. A very similar CNN architecture is used in [VvP23], where it is explained in more detail. The point is that all Mestre-Nagao sums inherently employ the same computation "rule" for each a_p, which we expect could be efficiently modeled by a matrix convolution operation. Thus, we can regard the training of a CNN as an optimization in the highly dimensional parameterized space of Mestre-Nagao-like heuristics.

Additionally, we use smaller fully connected neural networks (FCNN) for the classification of curves using only precomputed values of the selected Mestre-Nagao sums and conductors.

All described models are implemented in Python using the PyTorch library [PGM+19]. Our models' training and evaluation code is available online [KV22]. Models were trained using a server with dual Xeon 5218R CPUs (40 cores) equipped with 6 Nvidia Quadro RTX 5000 GPUs, each with 16 GB of RAM.

5.1. **Architecture of CNNs.** For each elliptic curve E, the CNN takes as an input a matrix $M(E)$ of shape $3 \times \pi(B)$, where $B = 10^3, 10^4, 10^5$ and the columns are indexed with primes less than B. The first row consist of a_p-s divided by $\sqrt{p}$ (by Hasse theorem $a_p/\sqrt{p} \in [-2, 2]$). The second row contains a constant sequence of normalized conductors, $\log N_E / \log N_{max}$, where N_{max} is the maximal conductor present in the dataset. The third row consists of a sequence of values $r_n = -1 + \frac{2n}{\pi(N)}$ (a linear sweep from -1 to 1). Each r_n represents the relative position of the n-th prime p_n in a sequence of primes less than B.

Each CNN consists of the following sequence of convolutional layers:

(1) Preparatory layer: increasing the number of channels (rows in the input matrix) from 3 to 64.
(2) Several input layers $I_1, \ldots, I_{L_1}$: preserving the number of channels and the length of the input sequence.
(3) Several reducing layers $R_1, \ldots, R_{L_2}$: preserving the number of channels and reducing the length of the input sequence by a factor of 2 (convolution kernel stride is equal to 2).
(4) Several output layers $O_1, \ldots, O_{L_3}$: preserving the number of channels and the length of the input sequence.

Each convolution layer is followed by an activation function and a batch normalization layer, improving the convergence of the network training and network generalization properties [IS15]. For the activation function, we decided to use ReLU. Kernel size KS is the same in each layer. The number of reducing layers L_2 is chosen such that the length of the output of the final reducing layer R_{L_2} (and consequently the length of the output of every output layer) is equal to 1.

Following convolutional layers, we have one final fully connected layer reducing dimensionality from 64 to the number of classification labels (ranks). Thus, our CNN architecture is fully determined with hyperparameters L_1, L_2, L_3, and KS. In contrast to model parameters, which are learned in the training process (see Section 5.3), hyperparameters are the parameters that determine the model architecture and the model optimization process.

For instance, in the case of uniform range for the LMFDB model with $p < 10,000$ we used the following values of hyperparameters: $L_1 = 0$, $L_2 = 11$, $L_3 = 3$, $KS = 17$. To find optimal values of hyperparameters we conducted Bayesian optimization [Moč75] in the space of hyperparameters by training altogether 500 different variants of networks. Similar hyperparameters were acquired for LMFDB in the case of $p < 1,000$ and for $p < 100,000$, due to lengthy computations, we just reused the hyperparameters for $p < 10,000$, by setting $L_2 = 14$. For each custom dataset CNN model, we took the same values of hyperparameters as for the corresponding LMFDB model.

5.2. **Architecture of FCNNs.** Here the input to the network for each curve E consists of one or more precomputed values of the Mestre-Nagao sums for a_p in a certain range and the normalized conductor N_E, as in the case of CNNs. In every case, our FCNN consists of an input linear layer having the size of the number of input features (the Mestre-Nagao sums and the normalized conductor), four hidden linear layers of size 128, and an output linear layer of the size of the number of classification labels (ranks). In between each of the linear layers, we use dropout [NHK$^+$14], which reduces overfitting during training, and the ReLU activation function. In our experience, the capacity of this network is more than enough to learn the dependency of rank on the input.

5.3. **Training procedure.** Training a neural network means optimizing network parameters (weights in convolutional and linear layers) to minimize a chosen loss function over a given dataset.

Dataset. For neural network training, as customary the whole dataset is divided into three disjoint subsets called training, validation, and test dataset. Only the training and validation datasets are used in network training. The training set is used directly by the gradient descent-based optimizer for the gradient backpropagation. The validation set is only used to avoid model overfitting or underfitting during training. The test dataset is not "seen" by the network during the training and is only used at the end to test the performance of already trained models. We used the $4 : 1$ ratio between the training and validation datasets.

Loss function. As we are training classifier networks, we decided to use the cross entropy loss function as implemented in PyTorch library [PGM$^+$19]. Additionally, we supply weights for the loss function to reflect on disproportional sizes of classes, which is considered standard practice.

Optimizer hyperparameters. Our models are trained using the fast.ai library [H$^+$18]. For the optimizer, we use the usual choice of Adam algorithm [KB17]. For governing learning rate and momentum scheduling we used a one-cycle policy with cosine annealing [ST18], which ensures better convergence of model parameters to a broad optimum and allows for better generalization of the trained model [Smi18]. For the optimizer hyperparameters, we used different ranges of the maximum learning rate for CNNs and FCNNs.

For CNNs the range was between $3.5 \cdot 10^{-4}$ and $1.5 \cdot 10^{-3}$. Number of training epochs was equal to 40, and batch size equal to 1024 ($p < 10^5$) or 2048 ($p < 10^3$ and $p < 10^4$). For Adam-specific hyperparameters, we have used: $\beta_2 = 0.99$, $\epsilon = 10^{-5}$, and weight decay of 10^{-3}.

For FCNNs, we employed Bayesian optimization for three hyperparameters: dropout, maximum learning rate, and weight decay, by training 200 different models (networks) for each of the 7 Mestre-Nagao sums $\{S_0, \ldots, S_6\}$ and also for Ω, in each of the 24 test variants. Finally, in each of these 192 tests performed, we took the model having the best MCC on the test set. The number of training epochs for every model was equal to 10 and the rest of the Adam-specific hyperparameters were the same as in the CNN training.

6. Results

We present rank classification results using the Mathews correlation coefficient in each of the 216 tests. We use two different datasets (LMFDB and custom, see Section 4), three a_p-s ranges ($p < 10^3, 10^4, 10^5$), two modes for selecting test curves (20% uniformly selected or top conductor range), and two types of classification (binary or all ranks).

For binary classification we always trained our networks for all ranks classification and to obtain binary classification we merged all rank labels into two categories, "low" and "high" ranks - effectively only reinterpreting all ranks classification, but rerunning Bayesian optimization for hyperparameters. For the LMFDB low ranks are $0, 1, 2, 3$ and high ranks are 4, and for the custom dataset low ranks are $0, \ldots, 7$ and high ranks are $8, 9, 10$. Interestingly, this procedure produced much better binary classification results than training directly a binary classifier model.

Regarding the CNN models, for each out of 12 test variants (varying two datasets, three ranges, and two modes for selecting test curves) we trained only 10 different networks due to high computational expense. For each of these 12 test variants, we computed the best MCC out of 10 different trained models, separately for all ranges classification and binary classification. For instance training of models in the worst case of $p < 10^5$ took over 14 hours per model on a single GPU. On the other hand, training of FCNNs for the Mestre-Nagao sums was much less computationally demanding, so for each of the 192 test cases, we trained at least 200 models (which took several minutes per model on a single GPU), using Bayesian optimization in the space of hyperparameters, as described in Section 5.3. For each of the test cases, we selected the best-performing model out of all trained models.

At the end of the section, we present the performance of the CNN model with $B = 10^5$ on a K3 elliptic surface dataset (see Section 4).

	Number of a_p-s used					
Type of	classify all ranks			binary classification		
classifier	$p < 10^3$	$p < 10^4$	$p < 10^5$	$p < 10^3$	$p < 10^4$	$p < 10^5$
CNN	**0.9507**	**0.9958**	**0.9992**	1	1	1
S_0	0.6823	0.8435	0.9068	0.9877	0.9758	0.9729
S_1	0.6848	0.8507	0.9301	0.9968	1	1
S_2	0.7277	**0.8697**	0.9359	0.9938	1	1
S_3	0.6933	0.8499	0.9142	0.9420	0.9842	0.9726
S_4	0.2678	0.3015	0.1525	0.2188	0.1103	0.0744
S_5	0.6132	0.7774	0.8463	0.9968	0.9968	1
S_6	**0.6969**	0.8647	**0.9381**	1	1	1
Ω	**0.8685**	**0.9602**	**0.9826**	1	1	1

TABLE 6. LMFDB with the uniform test dataset.

	Number of a_p-s used		
Type of	classify all ranks		
classifier	$p < 10^3$	$p < 10^4$	$p < 10^5$
CNN	**0.7564**	**0.9802**	**0.9961**
S_1	0.3498	0.6017	0.7552
Ω	0.5920	0.8203	0.9130

TABLE 7. LMFDB with the uniform test dataset and only prime conductors.

6.1. **LMFDB.** Test results for the complete LMFDB dataset are presented in Tables 6 and 10. As the LMFDB dataset is heterogeneous, we also separately present in Tables 7, 8, and 9 partial test results for all curves of prime conductor, all curves of conductor less than $500,000$, and all curves of prime conductor less than $500,000$, respectively.

In Table 6 are maximal values of the MCC obtained for different classifiers. Classifiers are trained using 80% of randomly selected curves from the LMFDB dataset, having a conductor less than 10^8. The MCC is computed on the other 20% of the dataset, not seen during the training. Classifiers (the CNN, Ω, and the Mestre-Nagao sums from Section 3) are trained using values of a_p-s for primes p less than 10^3, 10^4 or 10^5, and the value of the elliptic curve conductor.

For Tables 7, 8, and 9 we did not train additional classifiers. We evaluated already trained classifiers from Table 6 on the test dataset restricted to appropriate subsets.

In Table 10 classifiers are trained using all curves from the LMFDB dataset having a conductor less than 10^8. The MCC is computed on all curves from the LMFDB dataset having a conductor between 10^8 and 10^9, not seen during the training.

6.2. **Custom dataset.** Test results are presented in Tables 11 and 12.

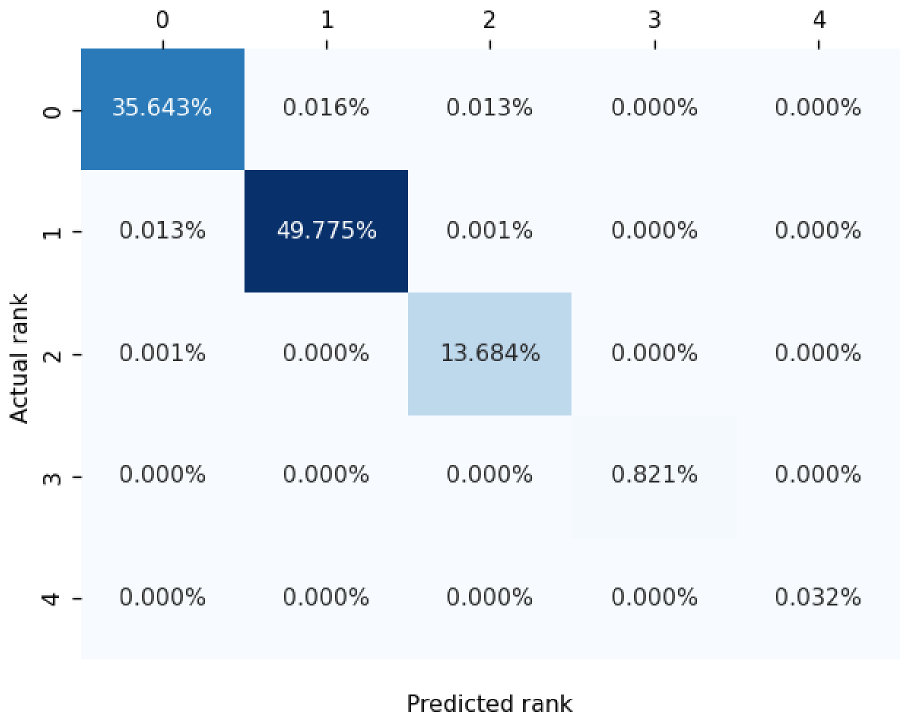

FIGURE 1. Confusion matrix of the CNN for the LMFDB and $p < 10^5$ with the uniform test dataset.

Type of classifier	Number of a_p-s used classify all ranks $p < 10^3$	$p < 10^4$	$p < 10^5$
CNN	**0.9838**	**0.9987**	**0.9998**
S_1	0.7413	0.8934	0.9602
Ω	0.9172	0.9831	0.9936

TABLE 8. LMFDB with the uniform test dataset and conductors less than $500,000$.

In Table 11 are maximal values of the MCC obtained for different classifiers. Classifiers are trained using 80% of randomly selected curves from the custom dataset with a conductor less than 10^{29}. As in the previous section, the MCC is computed on the other 20% of the dataset, not seen during the training.

In Table 12 classifiers are trained using all curves from the custom dataset with conductor less than 10^{29}. The MCC is computed on all curves from the custom dataset with conductor between 10^{29} and 10^{30}, not seen during the training.

	Number of a_p-s used		
Type of	classify all ranks		
classifier	$p < 10^3$	$p < 10^4$	$p < 10^5$
CNN	**0.9459**	**0.9985**	**1**
S_1	0.6535	0.8455	0.9392
Ω	0.9241	0.9633	0.9664

Table 9. LMFDB with the uniform test dataset and prime conductors less than $500,000$.

	Number of a_p-s used					
Type of	classify all ranks			binary classification		
classifier	$p < 10^3$	$p < 10^4$	$p < 10^5$	$p < 10^3$	$p < 10^4$	$p < 10^5$
CNN	**0.5631**	**0.9289**	**0.9846**	0.9811	0.9996	1
S_0	0.2880	**0.5057**	0.6545	0.9470	0.9750	0.9756
S_1	0.2791	0.4883	0.6658	0.9669	0.9996	1
S_2	0.2790	0.4968	**0.6730**	0.9609	0.9996	1
S_3	0.2897	0.5030	0.6574	0.9151	0.9716	0.9676
S_4	0.1352	0.1424	0.1850	0.2438	0.1411	0.0647
S_5	**0.2960**	0.3913	0.5261	0.9538	0.9917	0.9968
S_6	0.2632	0.4542	0.6416	0.9644	0.9996	1
Ω	**0.4433**	**0.7013**	**0.8530**	0.9796	1	1

Table 10. LMFDB with the top conductor range.

	Number of a_p-s used					
Type of	classify all ranks			binary classification		
classifier	$p < 10^3$	$p < 10^4$	$p < 10^5$	$p < 10^3$	$p < 10^4$	$p < 10^5$
CNN	**0.6129**	**0.7218**	**0.7958**	0.6695	0.8335	0.9425
S_0	0.5738	0.6782	0.7462	0.6761	0.8275	0.9175
S_1	**0.5780**	**0.6890**	**0.7592**	0.6484	0.8317	0.9309
S_2	0.5649	0.6761	0.7521	0.6407	0.8252	0.9206
S_3	0.5551	0.6616	0.7361	0.6515	0.8118	0.9074
S_4	0.2893	0.2472	0.2251	0.4271	0.4179	0.3874
S_5	0.4987	0.5990	0.6696	0.5230	0.6919	0.7956
S_6	0.5230	0.6509	0.7361	0.5179	0.7554	0.8961
Ω	**0.5999**	**0.7069**	**0.7807**	0.6821	0.8527	0.9412

Table 11. Custom dataset with the uniform test set

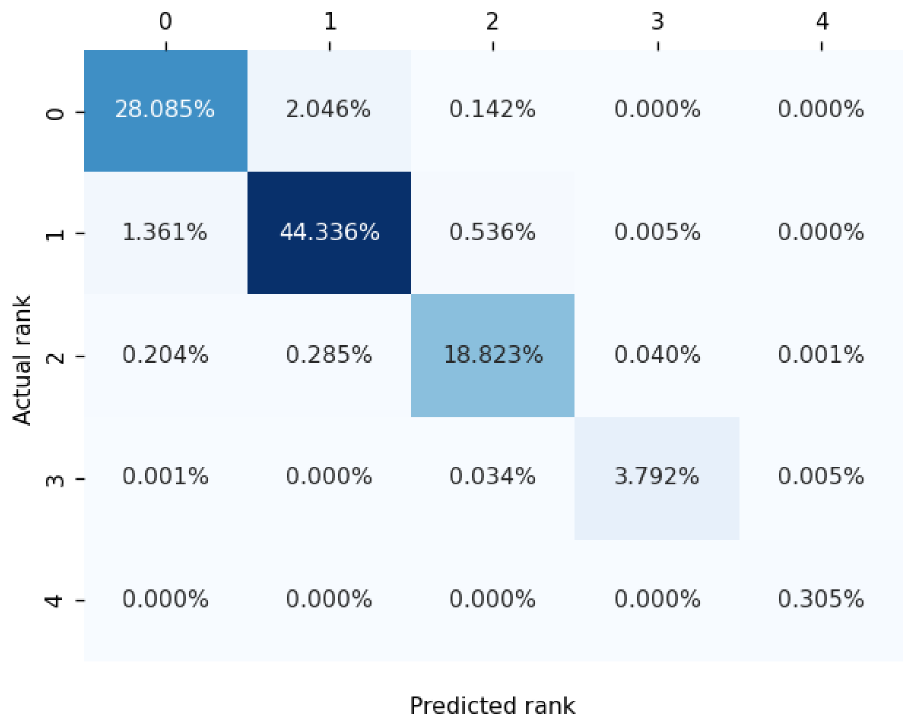

FIGURE 2. Confusion matrix of the CNN for the LMFDB and $p < 10^4$ with the top conductor range.

	Number of a_p-s used					
Type of classifier	classify all ranks			binary classification		
	$p < 10^3$	$p < 10^4$	$p < 10^5$	$p < 10^3$	$p < 10^4$	$p < 10^5$
CNN	0.2147	0.3019	0.3655	0.5449	0.6774	0.8082
S_0	0.2533	**0.3233**	**0.3719**	0.5866	0.6978	0.7900
S_1	**0.2573**	**0.3291**	**0.3834**	0.5649	0.6925	0.7946
S_2	0.2340	0.3118	0.3688	0.5472	0.6814	0.7856
S_3	**0.2556**	0.3189	0.3645	0.5688	0.6830	0.7807
S_4	0.1234	0.1228	0.1024	0.3966	0.3935	0.3842
S_5	0.2081	0.2858	0.3380	0.4860	0.6071	0.6880
S_6	0.1803	0.2757	0.3527	0.4321	0.6217	0.7326
Ω	**0.2622**	**0.3246**	**0.3905**	0.5931	0.7091	0.8118

TABLE 12. Custom dataset with the top conductor range.

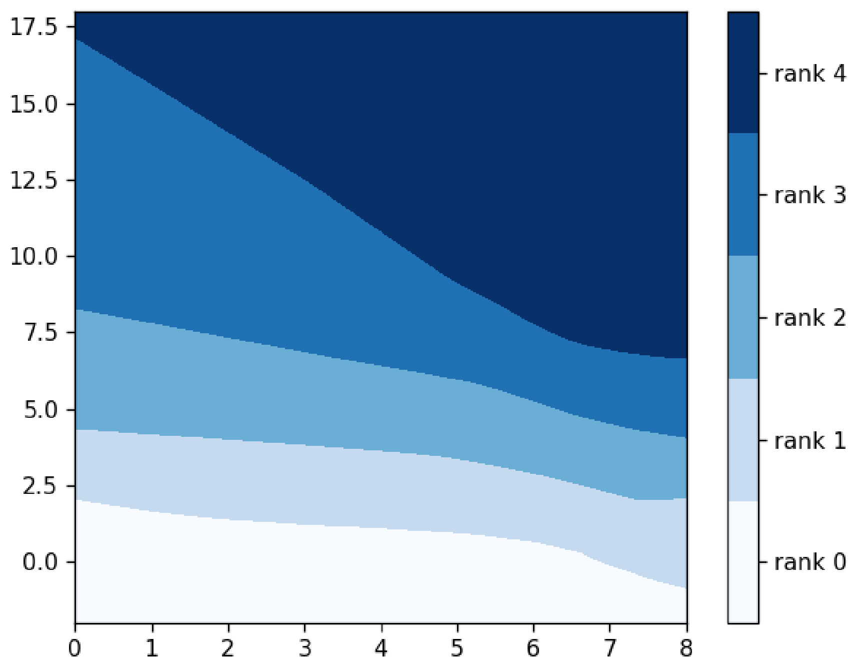

FIGURE 3. Rank cutoffs of the classifier S_5 as a function of a conductor, trained on the LMFDB with the uniform test set and $p < 10^4$. On the x-axis are $\log_{10}$ values of conductors and on the y-axis are values of the sum S_5. The unexpected shape of the cutoff between ranks 3 and 4 is the consequence of a small number of rank 4 curves with a small conductor, which are present in the dataset.

Figures 7 and 8 depict the relationship between the MCC and $\log_{10}(B\sqrt{N})$ for 82 subsets of curves corresponding to conductor intervals of $(1, 50000)$, $(50000 \cdot 2^k, 50000 \cdot 2^{k+1})$ for $k = 0, \ldots, 80$. In Figure 7, we present the results of the same CNN classifier for three different values of B (10^3, 10^4, and 10^5), while in Figure 8, we compare the performance of three different classifiers (the CNN, Ω, and S_1) for $B = 10^5$.

6.3. **K3 elliptic surface.** The confusion matrix of the CNN with $p < 10^5$ for this dataset can be found in Figure 9. The MCC of the CNN is equal to 0.2492.

6.4. **Discussion.** As expected, classifiers based on S_0, S_1, and S_2 have very similar performance across all tested regimes (improved convergence of sums S_1 and S_2 does not seem to improve the quality of the classification). They have the best performance of all considered Mestre-Nagao sums. Classifiers based on S_3 have an overall slightly

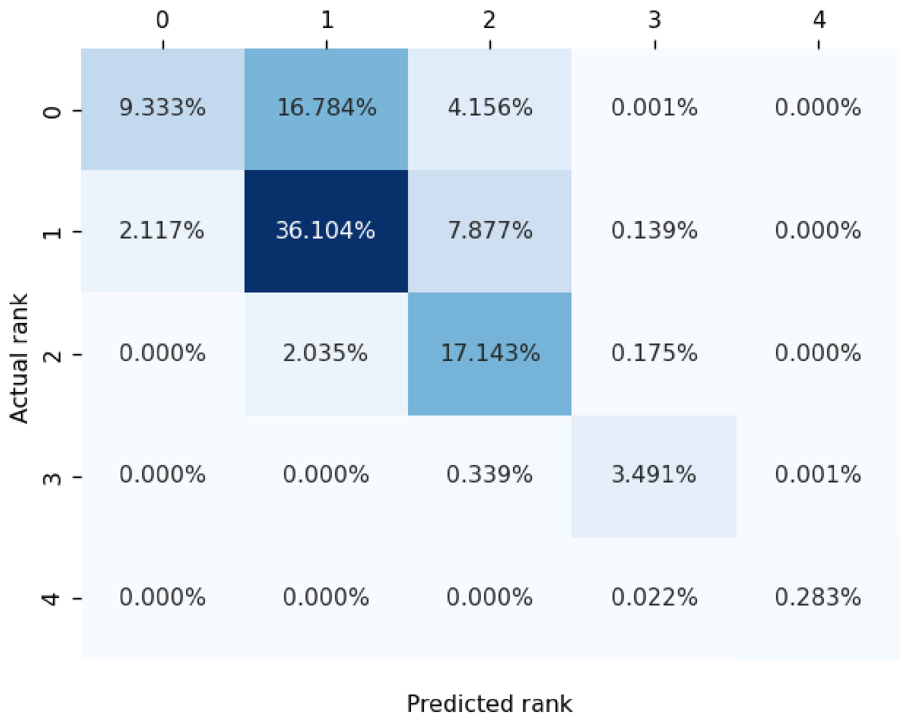

Actual rank \ Predicted rank	0	1	2	3	4
0	9.333%	16.784%	4.156%	0.001%	0.000%
1	2.117%	36.104%	7.877%	0.139%	0.000%
2	0.000%	2.035%	17.143%	0.175%	0.000%
3	0.000%	0.000%	0.339%	3.491%	0.001%
4	0.000%	0.000%	0.000%	0.022%	0.283%

FIGURE 4. Confusion matrix of S_0 for the LMFDB and $p < 10^4$ with the top conductor range.

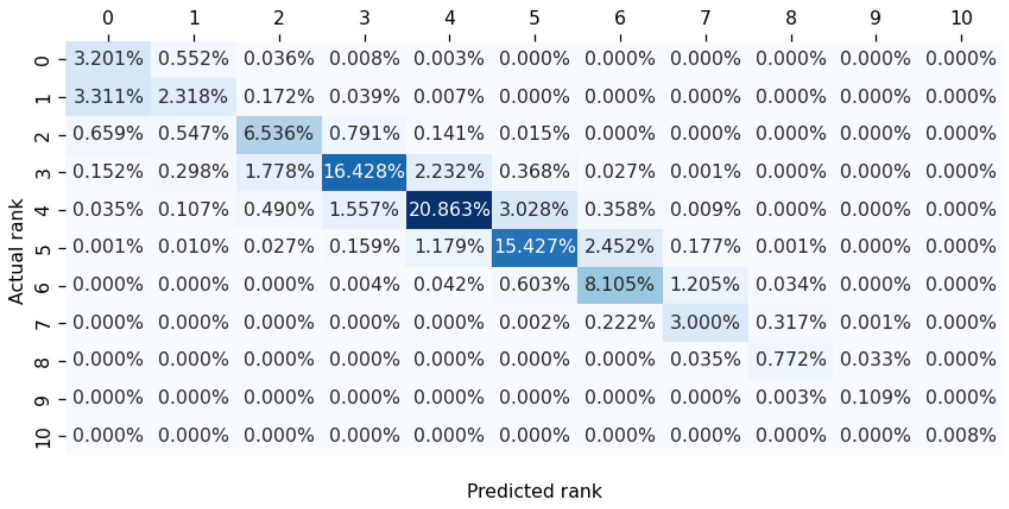

Actual rank \ Predicted rank	0	1	2	3	4	5	6	7	8	9	10
0	3.201%	0.552%	0.036%	0.008%	0.003%	0.000%	0.000%	0.000%	0.000%	0.000%	0.000%
1	3.311%	2.318%	0.172%	0.039%	0.007%	0.000%	0.000%	0.000%	0.000%	0.000%	0.000%
2	0.659%	0.547%	6.536%	0.791%	0.141%	0.015%	0.000%	0.000%	0.000%	0.000%	0.000%
3	0.152%	0.298%	1.778%	16.428%	2.232%	0.368%	0.027%	0.001%	0.000%	0.000%	0.000%
4	0.035%	0.107%	0.490%	1.557%	20.863%	3.028%	0.358%	0.009%	0.000%	0.000%	0.000%
5	0.001%	0.010%	0.027%	0.159%	1.179%	15.427%	2.452%	0.177%	0.001%	0.000%	0.000%
6	0.000%	0.000%	0.000%	0.004%	0.042%	0.603%	8.105%	1.205%	0.034%	0.000%	0.000%
7	0.000%	0.000%	0.000%	0.000%	0.000%	0.002%	0.222%	3.000%	0.317%	0.001%	0.000%
8	0.000%	0.000%	0.000%	0.000%	0.000%	0.000%	0.000%	0.035%	0.772%	0.033%	0.000%
9	0.000%	0.000%	0.000%	0.000%	0.000%	0.000%	0.000%	0.000%	0.003%	0.109%	0.000%
10	0.000%	0.000%	0.000%	0.000%	0.000%	0.000%	0.000%	0.000%	0.000%	0.000%	0.008%

FIGURE 5. Confusion matrix of the CNN for the custom dataset and $p < 10^4$ with the uniform test set.

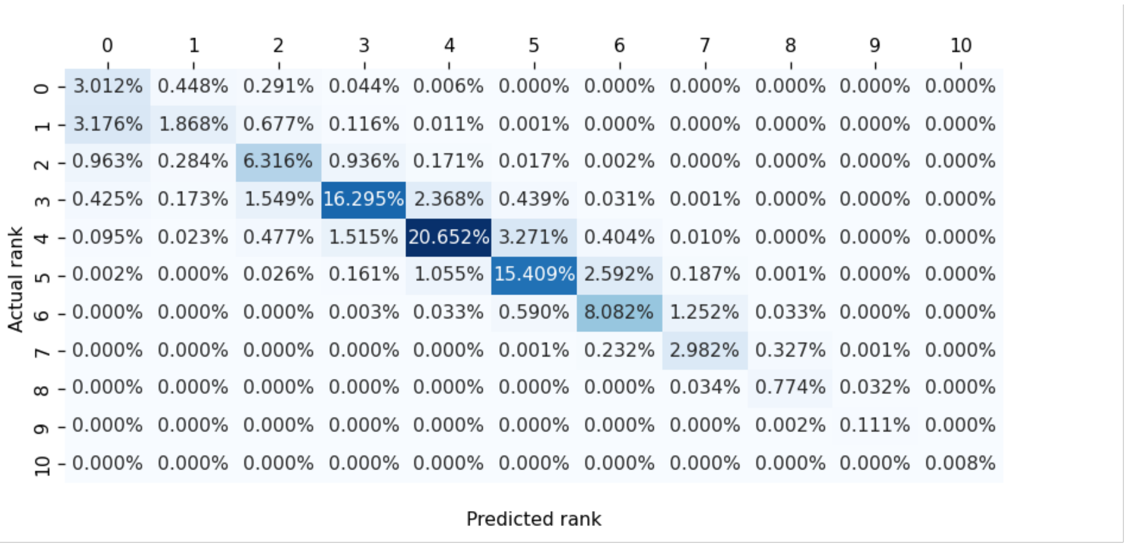

	0	1	2	3	4	5	6	7	8	9	10
0	3.012%	0.448%	0.291%	0.044%	0.006%	0.000%	0.000%	0.000%	0.000%	0.000%	0.000%
1	3.176%	1.868%	0.677%	0.116%	0.011%	0.001%	0.000%	0.000%	0.000%	0.000%	0.000%
2	0.963%	0.284%	6.316%	0.936%	0.171%	0.017%	0.002%	0.000%	0.000%	0.000%	0.000%
3	0.425%	0.173%	1.549%	16.295%	2.368%	0.439%	0.031%	0.001%	0.000%	0.000%	0.000%
4	0.095%	0.023%	0.477%	1.515%	20.652%	3.271%	0.404%	0.010%	0.000%	0.000%	0.000%
5	0.002%	0.000%	0.026%	0.161%	1.055%	15.409%	2.592%	0.187%	0.001%	0.000%	0.000%
6	0.000%	0.000%	0.000%	0.003%	0.033%	0.590%	8.082%	1.252%	0.033%	0.000%	0.000%
7	0.000%	0.000%	0.000%	0.000%	0.000%	0.001%	0.232%	2.982%	0.327%	0.001%	0.000%
8	0.000%	0.000%	0.000%	0.000%	0.000%	0.000%	0.000%	0.034%	0.774%	0.032%	0.000%
9	0.000%	0.000%	0.000%	0.000%	0.000%	0.000%	0.000%	0.000%	0.002%	0.111%	0.000%
10	0.000%	0.000%	0.000%	0.000%	0.000%	0.000%	0.000%	0.000%	0.000%	0.000%	0.008%

FIGURE 6. Confusion matrix of Ω for the custom dataset and $p < 10^4$ with the uniform test set.

worse performance than the first three sums. Peculiarly, S_4 underperforms in all tests, and its performance, in contrast to every other sum, decreases as the number of used a_p-s increases. Classifier S_5 performs well but compared to the first four sums is in most cases significantly lesser. While classifier S_6 is among the best on the curves having small conductors, its performance fades on larger conductors. Classifier Ω, which is based on all Mestre-Nagao sums simultaneously, is practically always better than any other sum-based classifier, especially on curves of a small conductor.

Finally, CNN-based classifiers on the LMFDB dataset were significantly better than Ω (and consequently any other sum-based classifier). On custom datasets with a uniform test set, they were slightly better than Ω and other classifiers, but on the custom dataset with top range conductor, they performed worse. Notice that every CNN-based classifier was selected as the best one out of only a 10 trained model, while each Mestre-Nagao sum-based classifier was selected out of at least 200 trained models, whose hyperparameters were additionally optimized using the Bayesian optimization technique. We expect that the quality of a CNN-based classification would increase with more trained models and possibly surpass other models. As the CNN model training is much more computationally expensive, more training was unfeasible for us. It is fascinating how the CNN almost perfectly classifies LMDFB with a uniform test database (see Figure 1) - it misclassified only 0.045% of all curves! On the other hand for the custom dataset, both the CNN and Ω classifiers perform similarly - their confusion matrices look almost identical (see Figures 5 and 6).

We noticed that all classifiers had the highest error rates when classifying curves of rank 0 and 1 (see Figure 5). Through the process of training Mestre-Nagao sum

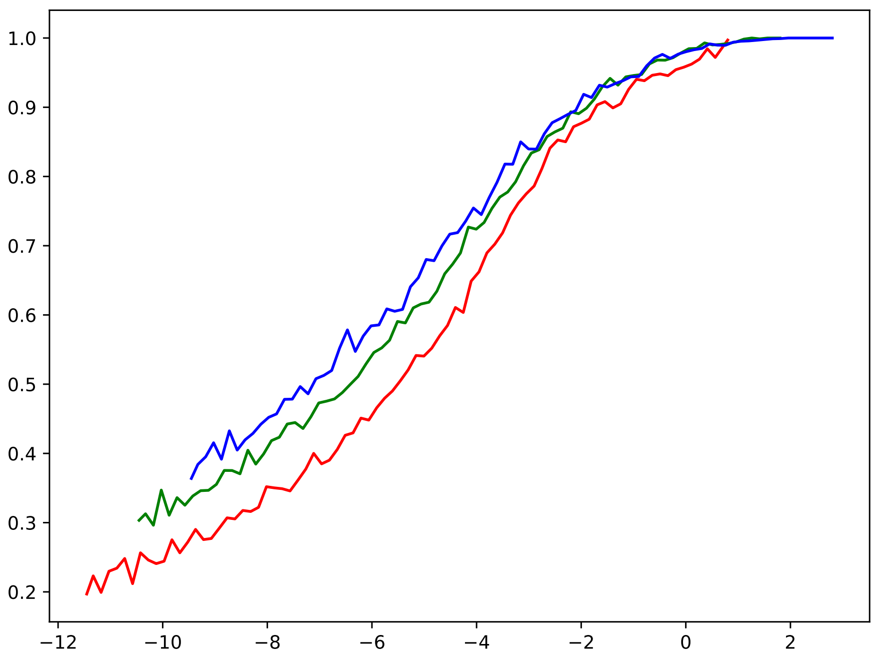

FIGURE 7. MCC of the CNN as a function of $\log_{10}(B/\sqrt{N})$, for $B = 10^3, 10^4, 10^5$ in red, green, and blue, respectively.

models, we were able to learn the optimal cutoffs for rank classification (see Figure 3). This information is particularly useful in searching for curves of high rank (as discussed in Section 7 of [EK20]).

Regarding the results presented in Tables 8 and 9, we noticed that classifying curves with prime conductors is more challenging than classifying all curves. This finding is surprising given our observation from the previous paragraph since the proportion of curves of rank 0 and 1 with prime conductors is lower than the proportion of curves of rank 0 and 1 in the entire LMFDB dataset. Notably, MCC values in Table 7 are significantly lower than the corresponding values for the entire LMFDB dataset, as the average conductor in the family of curves with a prime conductor is much higher than that in the LMFDB database.

As shown in Figure 8, the CNN outperforms the other two classifiers (S_1 and Ω) across the entire range of $B/\sqrt{N}$. For instance, to achieve an MCC level of 0.7, the CNN requires a B value that is approximately 6.5 times smaller than that required by the S_1 classifier for curves in the same conductor range.

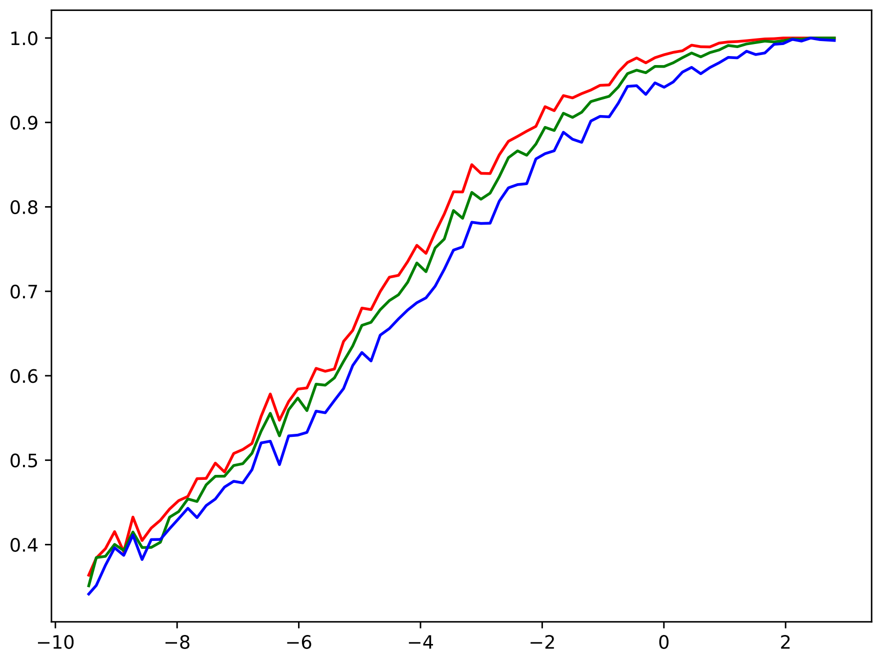

FIGURE 8. MCC as a function of $\log_{10}(B/\sqrt{N})$, for $B = 10^5$ and three different models: the CNN, Ω, and S_1 in red, green, and blue, respectively.

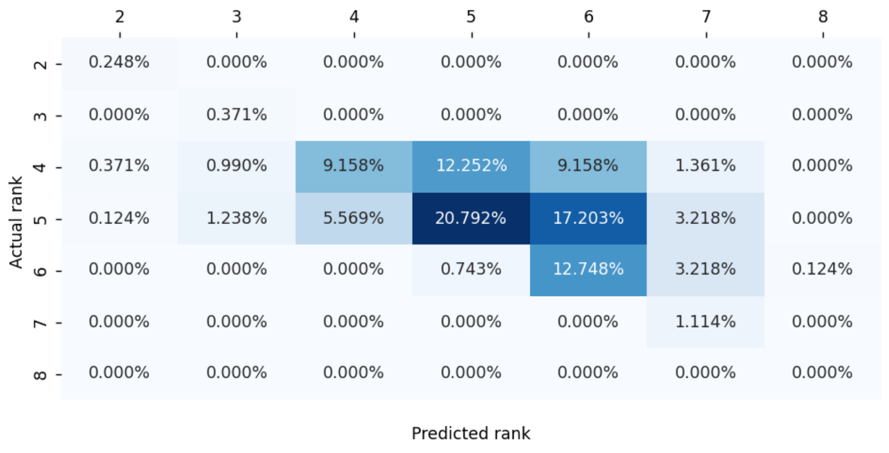

Actual rank \ Predicted rank	2	3	4	5	6	7	8
2	0.248%	0.000%	0.000%	0.000%	0.000%	0.000%	0.000%
3	0.000%	0.371%	0.000%	0.000%	0.000%	0.000%	0.000%
4	0.371%	0.990%	9.158%	12.252%	9.158%	1.361%	0.000%
5	0.124%	1.238%	5.569%	20.792%	17.203%	3.218%	0.000%
6	0.000%	0.000%	0.000%	0.743%	12.748%	3.218%	0.124%
7	0.000%	0.000%	0.000%	0.000%	0.000%	1.114%	0.000%
8	0.000%	0.000%	0.000%	0.000%	0.000%	0.000%	0.000%

FIGURE 9. Confusion matrix of the CNN for the K3 elliptic family and $p < 10^5$.

7. Future research

This paper left us with some open questions which may be addressed in future projects:

(1) The CNN and Ω models could be used as a substitution for the current use of the Mestre-Nagao sums in the search for elliptic curves of high rank. Also, these models could be trained on other elliptic curves datasets, such as curves with non-trivial torsion, and with additional input of the root number (to employ the Parity conjecture).

(2) It is unclear why the CNN works much better than all of the other Mestre-Nagao sum-based models on the curves from the LMFDB (or in general on curves of a small conductor). Did the CNN discover some new mathematics?

(3) Suboptimal choices in the CNN model architecture and optimizer hyperparameters (see Section 5) may lead to underperforming classifiers. One could perform more extensive optimization of hyperparameters, especially in the case of the custom dataset.

(4) Using some of the more advanced neural network architectures, originally developed for natural language processing tasks (see [VSP$^+$17]) may lead to better-performing models. The idea is that such architectures can more easily extract distant correlations in the a_p-s sequence.

Availability of data and materials

The data that support the findings of this study are available on request from the corresponding author M.K. The data are not publicly available due to the large size. The computer code that supports the findings of this study have been deposited at https://github.com/domagojvlah/deepellrank.

Conflict of interest

The authors declare that they have no conflict of interest.

Acknowledgments

We would like to express our sincere gratitude to the anonymous referees whose insightful comments and suggestions greatly improved the quality of the paper.

The first author was supported by the Croatian Science Foundation under the project no. IP-2018-01-1313, and by the QuantiXLie Center of Excellence, a project co-financed by the Croatian Government and European Union through the European Regional Development Fund - the Competitiveness and Cohesion Operational Programme (Grant KK.01.1.1.01.0004). The second author was supported by Croatian Science Foundation (HRZZ) grant PZS-2019-02-3055 from the "Research Cooperability" program funded by the European Social Fund.

References

[BCDT01] Christophe Breuil, Brian Conrad, Fred Diamond, and Richard Taylor. On the modularity of elliptic curves over $\mathbb{Q}$: wild 3-adic exercises. *J. Am. Math. Soc.*, 14(4):843–939, 2001.

[BJEA17] Sabri Boughorbel, Fethi Jarray, and Mohammed El-Anbari. Optimal classifier for imbalanced data using matthews correlation coefficient metric. *PLOS ONE*, 12(6):1–17, 06 2017.

[Bob13] Jonathan W. Bober. Conditionally bounding analytic ranks of elliptic curves. In *ANTS X—Proceedings of the Tenth Algorithmic Number Theory Symposium*, volume 1 of *Open Book Ser.*, pages 135–144. Math. Sci. Publ., Berkeley, CA, 2013.

[Boo05] Andrew R. Booker. Numerical tests of modularity. *J. Ramanujan Math. Soc.*, 20(4):283–339, 2005.

[BSS$^+$16] Andrew R. Booker, Jeroen Sijsling, Andrew V. Sutherland, John Voight, and Dan Yasaki. A database of genus-2 curves over the rational numbers. *LMS J. Comput. Math.*, 19(suppl. A):235–254, 2016.

[Cam99] Garikai Campbell. *Finding Elliptic Curves and Families of Elliptic Curves over $\mathbb{Q}$ of Large Rank*. PhD thesis, Rutgers University, 1999.

[Cas91] J. W. S. Cassels. *Lectures on elliptic curves*, volume 24 of *London Mathematical Society Student Texts*. Cambridge University Press, Cambridge, 1991.

[Coh15] Henri Cohen. Computing L-functions: a survey. *J. Théor. Nombres Bordeaux*, 27(3):699–726, 2015.

[DP21] Andrej Dujella and Juan Carlos Peral. Construction of high rank elliptic curves. *J. Geom. Anal.*, 31(7):6698–6724, 2021.

[Duj] Andrej Dujella. Infinite families of elliptic curves with high rank and prescribed torsion. `https://web.math.pmf.unizg.hr/~duje/tors/generic.html`.

[DVB$^+$21] A. Davis, P. Veličković, L. Buesing, et al. Advancing mathematics by guiding human intuition with ai. *Nature*, 600:70–74, 2021.

[EK20] Noam D. Elkies and Zev Klagsbrun. New rank records for elliptic curves having rational torsion. In *ANTS XIV. Proceedings of the fourteenth algorithmic number theory symposium, Auckland, New Zealand, virtual event, June 29 – July 4, 2020*, pages 233–250. Berkeley, CA: Mathematical Sciences Publishers (MSP), 2020.

[Elk06] Noam D. Elkies. Z^{28} in $E(\mathbb{Q})$. Number Theory Listserver, 2006.

[Elk07] Noam D. Elkies. Three lectures on elliptic surfaces and curves of high rank. arXiv:0709.2908, 2007.

[GBC16] Ian Goodfellow, Yoshua Bengio, and Aaron Courville. *Deep Learning*. MIT Press, 2016. `http://www.deeplearningbook.org`.

[Gol82] Dorian Goldfeld. Sur les produits partiels eulériens attachés aux courbes elliptiques. *C. R. Acad. Sci. Paris Sér. I Math.*, 294(14):471–474, 1982.

[H$^+$18] Jeremy Howard et al. fastai. `https://github.com/fastai/fastai`, 2018.

[HLO23] Yang-Hui He, Kyu-Hwan Lee, and Thomas Oliver. Machine learning invariants of arithmetic curves. *J. Symbolic Comput.*, 115:478–491, 2023.

[HLOP22] Yang-Hui He, Kyu-Hwan Lee, Thomas Oliver, and Alexey Pozdnyakov. Murmurations of elliptic curves. arXiv:2204.10140, 2022.

[IS15] Sergey Ioffe and Christian Szegedy. Batch normalization: Accelerating deep network training by reducing internal covariate shift, 2015. cite arxiv:1502.03167.

[IV21] Tomislav Ivek and Domagoj Vlah. BlackBox: generalizable reconstruction of extremal values from incomplete spatio-temporal data. *Extremes*, 24(1):145–162, 2021.

[IV23] Tomislav Ivek and Domagoj Vlah. Reconstruction of incomplete wildfire data using deep generative models. *Extremes*, 2023.

[KB17] Diederik P. Kingma and Jimmy Ba. Adam: A method for stochastic optimization, 2017.

[KM22] Seoyoung Kim and M. Ram Murty. From the Birch and Swinnerton-Dyer conjecture to Nagao's conjecture. to appear in Math. Comp., 2022. With an appendix by Andrew V. Sutherland.

[KS08] Kiran S. Kedlaya and Andrew V. Sutherland. Computing L-series of hyperelliptic curves. In *Algorithmic number theory*, volume 5011 of *Lecture Notes in Comput. Sci.*, pages 312–326. Springer, Berlin, 2008.

[KSH12] Alex Krizhevsky, Ilya Sutskever, and Geoffrey E. Hinton. Imagenet classification with deep convolutional neural networks. *Advances in Neural Information Processing Systems*, 25:1106–1114, 2012.

[KV22] Matija Kazalicki and Domagoj Vlah. deepellrank. `https://github.com/domagojvlah/deepellrank`, 2022.

[LMF22] The LMFDB Collaboration. The L-functions and modular forms database. `http://www.lmfdb.org`, 2022. [Online; accessed 4 July 2022].

[Maz77] B. Mazur. Modular curves and the Eisenstein ideal. *Publ. Math., Inst. Hautes Étud. Sci.*, 47:33–186, 1977.

[Mes82] Jean-François Mestre. Construction d'une courbe elliptique de rang ≥ 12. *C. R. Acad. Sci., Paris, Sér. I*, 295:643–644, 1982.

[Moč75] J. Močkus. *On Bayesian Methods for Seeking the Extremum*, pages 400–404. Springer Berlin Heidelberg, Berlin, Heidelberg, 1975.

[Nag92] Koh-ichi Nagao. Examples of elliptic curves over $\mathbb{Q}$ with rank ≥ 17. *Proc. Japan Acad., Ser. A*, 68(9):287–289, 1992.

[NHK$^+$14] Srivastava Nitish, Geoffrey Hinton, Alex Krizhevsky, Ilya Sutskever, and Ruslan Salakhutdinov. Dropout: A simple way to prevent neural networks from overfitting. *Journal of Machine Learning Research*, 15(56):1929–1958, 2014.

[Par19] *PARI/GP, version* `2.11.1`. Bordeaux, 2019. `http://pari.math.u-bordeaux.fr/`.

[PGM$^+$19] Adam Paszke, Sam Gross, Francisco Massa, Adam Lerer, James Bradbury, Gregory Chanan, Trevor Killeen, Zeming Lin, Natalia Gimelshein, Luca Antiga, Alban Desmaison, Andreas Köpf, Edward Yang, Zachary DeVito, Martin Raison, Alykhan Tejani, Sasank Chilamkurthy, Benoit Steiner, Lu Fang, Junjie Bai, and Soumith Chintala. Pytorch: An imperative style, high-performance deep learning library. In Hanna M. Wallach, Hugo Larochelle, Alina Beygelzimer, Florence d'Alché-Buc, Emily B. Fox, and Roman Garnett, editors, *Advances in Neural Information Processing Systems 32: Annual Conference on Neural Information Processing Systems 2019, NeurIPS 2019, 8-14 December 2019, Vancouver, BC, Canada*, pages 8024–8035, 2019.

[Poi01] H. Poincaré. Sur les propriétés arithmétiques des courbes algébriques. *Journ. de Math. (5)*, 7:161–233, 1901.

[PPVW19] Jennifer Park, Bjorn Poonen, John Voight, and Melanie Matchett Wood. A heuristic for boundedness of ranks of elliptic curves. *J. Eur. Math. Soc. (JEMS)*, 21(9):2859–2903, 2019.

[S$^+$11] William A. Stein et al. *Purple SAGE*, 2011. `http://purple.sagemath.org/`.

[Smi18] Leslie N. Smith. A disciplined approach to neural network hyper-parameters: Part 1 – learning rate, batch size, momentum, and weight decay, 2018.

[ST18] Leslie N. Smith and Nicholay Topin. Super-convergence: Very fast training of neural networks using large learning rates, 2018.

[VSP$^+$17] Ashish Vaswani, Noam Shazeer, Niki Parmar, Jakob Uszkoreit, Llion Jones, Aidan N Gomez, Łukasz Kaiser, and Illia Polosukhin. Attention is all you need. In I. Guyon, U. Von Luxburg, S. Bengio, H. Wallach, R. Fergus, S. Vishwanathan, and R. Garnett, editors, *Advances in Neural Information Processing Systems*, volume 30. Curran Associates, Inc., 2017.

[VvP23] Domagoj Vlah, Karlo Šepetanc, and Hrvoje Pandžić. Solving bilevel optimal bidding problems using deep convolutional neural networks. *IEEE Systems Journal*, pages 1–12, 2023.

[Wag21] Adam Z. Wagner. Constructions in combinatorics via neural networks. arXiv:2104.14516, 2021.

[Wat15] Mark Watkins. A discursus on 21 as a bound for ranks of elliptic curves over q, and sundry related topics. `http://magma.maths.usyd.edu.au/~watkins/papers/DISCURSUS.pdf`, 2015.

[WDE+14] Mark Watkins, Stephen Donnelly, Noam D. Elkies, Tom Fisher, Andrew Granville, and Nicholas F. Rogers. Ranks of quadratic twists of elliptic curves. In *Numéro consacré au trimestre "Méthodes arithmétiques et applications", automne 2013*, pages 63–98. Besançon: Presses Universitaires de Franche-Comté, 2014.

[Wil95] Andrew Wiles. Modular forms, elliptic curves, and Fermat's Last Theorem. In *Proceedings of the international congress of mathematicians, ICM '94, August 3-11, 1994, Zürich, Switzerland. Vol. I*, pages 243–245. Basel: Birkhäuser, 1995.

Department of Mathematics, University of Zagreb, Bijenička cesta 30, 10000 Zagreb, Croatia
Email address: `matija.kazalicki@math.hr`

Department of Applied Mathematics, Faculty of Electrical Engineering and Computing, University of Zagreb, Unska 3, 10000 Zagreb, Croatia
Email address: `domagoj.vlah@fer.hr`